Conformational Analysis and Molecular Dynamics Simulation of Lactose

Jaetaek Oh, Yangmee Kim*, and Youngdo Won

Department of Chemistry, Hanyang University, Seoul, Korea
**Department of Chemistry, Konkuk University, Seoul, Korea*
Received June 26, 1995

The conformational details of β-lactose are investigated through molecular dynamics simulations in conjunction with the adiabatic potential energy map. The adiabatic energy map generated *in vacuo* contains five local minima. The lowest energy structure on the map does not correspond to the structure determined experimentally by NMR and the X-ray crystallography. When aqueous solvent effect is incorporated into the energy map calculation by increasing the dielectric constant, one of the local minima in the vacuum energy map becomes the global minimum in the resultant energy map. The lowest energy structure of the energy map generated *in aquo* is consistent with the one experimentally determined. Molecular dynamics simulations starting from those five local minima on the vacuum energy map reveal that conformational transitions can take place among various conformations. Molecular dynamics simulations of the lactose and ricin B chain complex system in a stochastic boundary indicate that the most stable conformation in solution phase is bound to the binding site and that there are conformational changes in the exocyclic region of the lactose molecule upon binding.

Introduction

Control of important biological processes as growth and defence against invading organisms, requires that a cell interacts with its environment at the level of its external membrane surface. These interactions often involve the binding of a protein to an oligosaccharide receptor anchored to the membrane as a part of an integral glycoprotein or glycolipid. Lectin offers excellent models for the study of protein-carbohydrate interactions.[1,2] For example, the ricin B chain recognizes galactose-terminated oligosaccharides such as lactose and melibiose specifically at the membrane surface.[3~5] According to the previous NMR study it is found that free lactose and free melibiose exist with a variety of conformational flexibility and there are considerable conformational changes of melibiose induced by binding to ricin. It suggests the tendency of protein binding to restrict conformational freedom about the glycosidic bond.[6,7] In order to understand the structural details of such protein-carbohydrate interactions it is necessary to study the structural changes of oligosaccharide as a recognition signal. Here, the flexibilities in the structure of lactose which can be a receptor for protein at the membrane surface are studied using the adiabatic potential energy map and molecular dynamics simulations.

Lactose (4-o-β-D-galactopyranosyl-β-D-glucopyranoside) contains the β (1→4) linkage and consequently possesses two variable torsion angles, φ and ψ, about the glycosidic linkage. Therefore, most conformational analyses of carbohydrates have been carried out with changing mainly the glycosidic torsion angles. In theoretical studies on oligosaccharide structures, it is often assumed that the pyranose ring of monomer is rigid and most internal coordinates are fixed during the conformational search.[8] Although this is a useful approximation, there are many evidences to point out the importance of internal flexibility in predicting stable conformations of polysaccharides.[9~13] Because the accumulation of small changes in the internal coordinates often avoids significant steric conflicts, adiabatic energy calculations result in enlarged thermally accessible conformational space.[14] In the present study, we have carried out the conformational analysis of lactose with complete internal flexibility. The great number of degrees of freedom in a complex conformational space entails the multiple minimum problem, which is overcome through thorough and systematic energy minimizations to generate the adiabatic energy map. In order to account on the aqueous solvent effect, dielectric shielding is also incorporated into the potential energy calculation through an effective dielectric constant.

Theory and Computational Method

Molecular Mechanical Potential. The standard CHARMM (Chemistry at HARvard Macromolecular Mechanics)[15] potential energy function is used to model the lactose molecule and the ricin B chain.

$$\begin{aligned} V(q) = & \sum k_{b_i}(r_i - r_i^0)^2 + \sum k_{\theta_i}(\theta_i - \theta_i^0)^2 \\ & + \sum k_{UB_i}(s_i - s_i^0)^2 + \sum k'_{UB_i}(s_i - s_i^0) \\ & + \sum k_{\phi_i}[1 + \cos(n_i\phi_i - \delta_i)] + \sum k_{\omega_i}(\omega_i - \omega_i^0)^2 \\ & + \sum\left(\frac{A_{ij}}{r_{ij}^{12}} - \frac{B_{ij}}{r_{ij}^{6}}\right) + \sum \frac{q_i q_j}{4\pi\varepsilon_0 r_{ij}} \end{aligned} \quad (1)$$

The potential includes harmonic terms for bond stretching, bond angle bending, Urey-Bradley 1-3 interaction and improper torsion energies. The dihedral energy terms take the cosine form with the force constant k_ϕ, the periodicity n and the phase factor δ. Nonbonding (1-4 or further separated) interaction energy includes van der Waals and electrostatic terms. Note that hydrogen bond energy terms are not explicitly included but treated as nonbonding interactions in the CHARMM potential.

Hydrogen atoms are explicitly included in the molecular

Table 1. Atomic Parameters of the Lactose Molecular Model

Atom type	Mass	Description	van der Waals parameter	
			ε	σ
HA	1.0080	Non-polar hydrogen	−0.0420	1.330
HO	1.0080	Polar hydrogen	−0.0948	0.760
CT	12.0110	Aliphatic sp^3 carbon	−0.0903	1.800
OE	15.9994	Ether oxygen	−0.1591	1.600
OT	15.9994	Hydroxyl oxygen	−0.1521	1.550

Atom Type and Atomic Charge

Atom	Type	Charge	Atom	Type	Charge	Atom	Type	Charge
C1′	CT	0.311	H5′	HA	0.046	C3	CT	0.201
H1′	HA	0.031	O5′	OE	−0.370	H3	HA	0.071
C2′	CT	0.201	C6′	CT	0.180	O3	OT	−0.650
H2′	HA	0.071	H6a′	HA	0.050	HO3	HO	0.400
O2′	OT	−0.650	H6b′	HA	0.050	C4	CT	0.141
HO2′	HO	0.400	O6′	OT	−0.650	H4	HA	0.071
C3′	CT	0.201	HO6′	HO	0.400	O4	OE	−0.380
H3′	HA	0.071	C1	CT	0.371	C5	CT	0.076
O3′	OT	−0.650	H1	HA	0.031	H5	HA	0.046
HO3′	HO	0.400	O1	OT	−0.650	O5	OE	−0.370
C4′	CT	0.201	HO1	HO	0.400	C6	CT	0.180
H4′	HA	0.071	C2	CT	0.201	H6a	HA	0.050
O4′	OT	−0.650	H2	HA	0.071	H6b	HA	0.050
HO4′	HO	0.400	O2	OT	−0.650	O6	OT	−0.650
C5′	CT	0.076	HO2	HO	0.400	HO6	HO	0.400

model following the all-hydrogen parameter set of CHARMM version 22. The CHARMM protein parameter set is employed in modeling the ricin B chain. The parameters of the lactose molecule are obtained from the CHARMm version 22 parameter set[16] and listed in Table 1 and 2. The similar set of parameters for carbohydrates is also available through QUANTA.[17] Figure 1 shows the atom naming scheme of the lactose molecule constructed by linking the galactose and the glucose moieties through the β(1→4) glycosidic bond. Molecular mechanical parameters of the lactose model are listed in Table 1 and 2. The parameter set has high atomic partial charges to treat the increased polarization of the hydroxyl group forming multiple hydrogen bonds in solution. The parameters for the glycosidic linkage are adopted from those used for the ring C5-O5-C1 ether linkage.

Solvent Effects. It is of primary interests to investigate conformational detail of lactose in an aqueous medium. Solution phase simulations have been major applications of molecular dynamics. With proper boundary conditions, either periodic[18] or stochastic,[19] one can easily perform molecular dynamics simulations of lactose in the aqueous solvent which is composed of explicit water molecules such as TIP3P[20] and ST2.[21] However, such molecular dynamics simulations are inefficient in navigating the entire conformational space. One would not observe many conformational changes enough to sample all representative conformers in a reasonable simulation time (e.g., 1 or 2 ns). Furthermore, there is no feasible way to carry out energy map calculations with the lactose molecule in the solvent environment of explicit water molecules.

Table 2. Molecular Mechanical Parameters of the Lactose Molecular Model

Bond parameters			Dihedral parameters			
Bond type	k_b	r^0	Dihedral Type	k_ϕ	n	δ
CT-CT	268.0	1.529	CT-CT-CT-CT	0.70	1	0.0
CT-OT	375.0	1.405	CT-CT-CT-CT	0.13	3	0.0
CT-OE	390.0	1.407	CT-CT-CT-OE	0.55	1	0.0
HA-CT	340.0	1.090	CT-CT-CT-OT	0.65	1	0.0
HO-OT	505.0	0.948	CT-CT-OE-CT	0.82	1	0.0
			CT-CT-OE-CT	0.25	3	0.0
Angle Parameters			CT-CT-OT-HO	0.35	1	0.0
Angle Type	k_θ	θ^0	CT-CT-OT-HO	0.35	3	0.0
CT-CT-CT	58.35	112.7	HA-CT-OT-HO	0.05	3	0.0
CT-CT-OT	45.00	110.5	OE-CT-OE-CT	1.30	1	180.0
CT-OE-CT	58.00	112.4	OE-CT-OT-HO	1.50	1	180.0
HA-CT-CT	37.50	110.7	OE-CT-OT-HO	0.65	3	0.0
HA-CT-OE	55.50	109.5	OT-CT-CT-OT	3.43	1	0.0
HA-CT-HA	33.00	107.8	OT-CT-CT-OT	1.70	3	0.0
HA-CT-OT	55.00	108.0	X-CT-CT-X	0.15	3	0.0
HO-OT-CT	59.00	106.7	X-CT-OE-X	0.27	3	0.0
OE-CT-OT	48.00	107.8	X-CT-OT-X	0.25	3	0.0
CT-CT-OE	57.00	110.0				
OE-CT-OE	60.00	109.0				

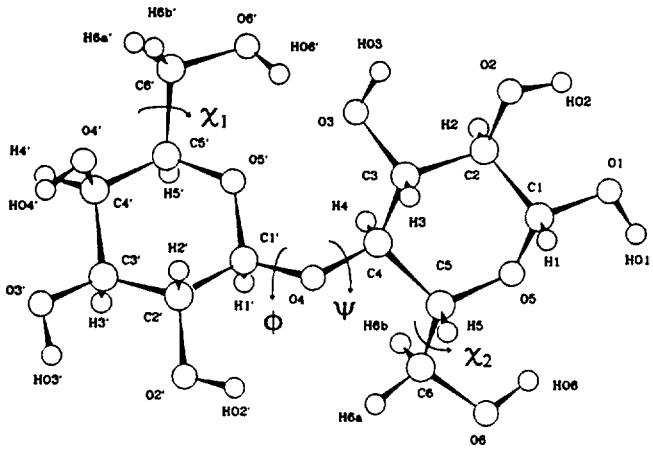

Figure 1. The atom naming scheme of the lactose molecule. The glycosidic dihedral angles, Φ and Ψ, are defined with H1′-C1′-O4-C4 and C1′-O4-C4-H4, respectively.

In the molecular mechanical potential of Eq. (1), the dielectric medium effect can be incorporated into the electrostatic energy terms through the dielectric constant. The constant dielectric or the distance scaled dielectric options are normally used with the dielectric constant = 1.0 when explicit solvent molecules are included in the energy calculation. Without explicit solvent molecules, the medium effect of dielectric screening can be effectively mimicked by increasing the dielectric constant. In this work, several dielectric constants, ε = 1.0, 4.0, 10.0 and 50 are employed in a series of energy map generations and molecular dynamics simulations.

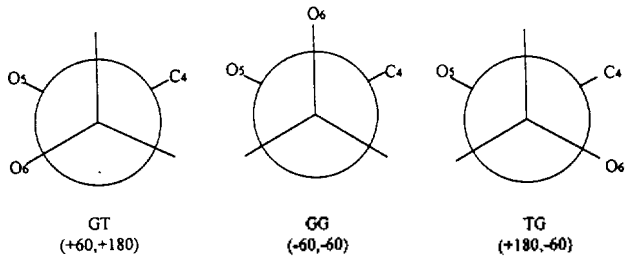

Figure 2. Definition of exocyclic conformations of a six membered sugar ring. The numbers in parentheses refer to the torsion angles O5-C5-C6-O6 and C4-C5-C6-O6, respectively.

$\varepsilon = 1.0$ is the vacuum value, 4.0 is known to be that for protein medium. We note that the electrostatic energy is a slow varing function of the dielectric constant above $\varepsilon = 10.0$.

Adiabatic Energy Map. The relative orientation of the monosaccharide units of (1→4)-linked disaccharides can be described by the two torsional angles of the glycosidic linkage. In Figure 1, the glycosidic torsional angles ϕ and ψ are defined as H1'-C1'-O4-C4 and C1'-O4-C4-H4, respectively. The disaccharide conformational energy can be mainly described in terms of the variation of the molecular energy as a function of the glycosidic torsional angles. The conformational energy surface is constructed in the (ϕ, ψ) space as a contour map.

In general, conformational analyses of a molecule with as many degrees of freedom as lactose are complicated with multiple local minima on the complex multidimensional energy hypersurface. Conventional energy minimization methods applied to a grid point in the (ϕ, ψ) space do not warrant that the resultant structure is the lowest energy structure corresponding to the grid point. Because energy barriers between local minima are not overcome during the energy minimization procedure, a system normally relaxes to the nearest local minimum. As there is no general solution available to the multiple minimum problem, we have carried out numerous minimizations for a set of systematically selected initial geometries.

Two structural arrangements are found important in analyzing the conformational energy as a function of the glycosidic torsion angles: the orientation of the exocyclic hydroxymethyl groups and the intraring hydrogen bonding pattern. Three possible exocyclic hydroxymethyl group orientations relative to O5 and C4 are designated GT(60, 180), GG(-60, 60) and TG(180, -60) as depicted in Figure 2.[22] Due to strong electrostatic interactions, hydroxyl groups in a monosaccharide ring form hydrogen bonds among themselves with all the OH vectors pointing the same direction around the ring. With numbering of carbon atoms increasing clockwise, a clockwise pattern of intraring hydrogen bonding is designated "C". A reverse clockwise pattern is designated "R". A minimization procedure is initiated from the structures prepared for each (ϕ, ψ) grid point with considering these conformational aspects.

The adiabatic potential energy map is generated as follows.[22] First, monomer conformations of glucose and galactose are studied with paying special attentions to the orientation of hydroxyl groups. Because hydrogen bonds can be stabilized in either R or C form around the ring, both conformations are considered in preparing initial geometries. Multiple minimizations are performed on the initial geometries of both R and C forms with the exocyclic hydroxymethyl group rotated by 30° increments. Thus minimized structures are adopted into the internal coordinate (IC) entries of the residue definition in the residue topology file (RTF) so that they may be utilized in generating lactose initial geometries.

The minimized conformations of glucose and galactose are patched to generate the initial geometries of lactose at each grid point in the (ϕ, ψ) space. There are four possible combinations of monomeric saccharide ring conformations in regards to the intraring hydrogen bonding arrangements: RR, RC, CR, and CC. As three exocyclic hydroxymethyl group orientations are also considered, there are nine possible conformations for each dimeric combination and a total of 36 initial geometries are considered for each grid point. The grid in the (ϕ, ψ) space is constructed with 20° in spacing. Each combined structural conformation at a grid point is initially minimized with the steepest descent (SD) minimizer for 100 steps and subsequently with the adopted basis Newton-Raphson (ABNR) minimizer until the root-mean-square (rms) gradient becomes less than 0.01 kcal/mole Å. All degrees of freedom are relaxed from the initial geometry except the glycosidic torsional angles, which are fixed to the grid point ϕ and ψ values. The lowest energy structure out of 36 minimized ones is taken to be the conformation at the grid point. A total of 19×19 energy values are obtained for the energy map with 20° spacing, on which local minima can be located.

The energy contour on the 19×19 grid is finally refined around each local minimum. Additional points are layed with increments of 5° in ϕ and ψ away each local minimum and further minimizations are performed on those points to optimize the energy contour. The same procedure is used to generate adiabatic energy maps with the a spectrum of dielectric constants employed in this work.

Molecular Dynamics Simulation. Having prepared the adiabatic energy map, molecular motions of the lactose molecule at the room temperature are examined through a series of molecular dynamics simulations. Each dynamics trajectory is initiated from one of the local minima on the adiabatic energy map and the equations of motion are integrated with the Verlet integrator[23] of CHARMM. As hydrogen containing bond lengths are fixed by the SHAKE algorithm during the integration, 1fs time step is appropriate for the dynamics run.

The following standard molecular dynamics simulation protocol is employed and conformational changes are monitored during the simulation. First, the molecule with a local minimum conformation is heated to the simulation temperature (300 K) with increasing the temperature by 2 K in every 50 fs of dynamics. At each 50 fs step, the atomic velocities are reassigned according to the Gaussian random deviates corresponding to the temperature. Then, the system is equilibrated for 10 ps with scaling atomic velocities periodically (every 50 fs) if the temperature is deviated from the simulation temperature by more than 5 K. After the equilibration, the equations of motion are integrated without velocity rescaling for additional 20 ps. During the 20 ps production

phase dynamics run, the total energy is checked well conserved.

The lactose model system is an isolated molecule and has relatively small number of degrees of freedom. As it moves around the phase space very fast, conformational changes can take place at an early stage of dynamics simulation. Therefore, it is necessary to monitor the entire dynamics trajectory of the lactose molecule from the heating phase.

Molecular Dynamics Simulation of the Lactose-Ricin B Complex. The conformational behavior of lactose upon binding to the ricin B chain is also examined through the dynamics simulation of the lactose-ricin B complex. The X-ray crystallographic structure of the ricin B chain has been determined at 2.5 Å resolution. It shows that the ricin B chain contains two β-galactose-specific noncooperative binding sites with slightly different binding affinities.[4] Here, we call them site 1 and site 2 respectively. In order to investigate the conformation of the lactose bound to the ricin, separate molecular dynamics simulations are carried out for each lactose binding site under a stochastic boundary condition.

The lactose molecule bound to a binding site is placed at the center of the 15 Å radius sphere, which is to contain all atoms considered in the stochastic boundary molecular dynamics (SBMD) simulation. Another sphere with the radius of 13 Å is concentrically placed to surround the reaction region. The volume in between 13 Å and 15 Å radius is called the buffer region. While atoms in the reaction region are subject to the normal dynamics, *i.e.*, Newtonian equations of motion, atoms in the buffer region are treated by Langevin dynamics with the Langevin friction and the stochastic mean field approximation. All atoms outside the 15 Å sphere (called the reservoir region) comprise the heat bath and interact with those atoms in the reaction and the buffer regions through Langevin forces. Reservoir region atoms are considered to be fixed and excluded from the dynamics integration, which reduces the size of the system to a few thousand atoms.

Once the ricin B chain moiety and the lactose molecule are placed in the stochastic boundary, TIP3P water molecules are introduced to solvate the lactose-ricin complex. A water sphere with the radius larger than 15 Å is placed concentrically with the reaction region sphere and water molecules overlapping with the solute are removed. Water molecules are subject to a stochastic boundary potential in addition to the molecular mechanical potential described in Eq. (1). Bulk water orientations are optimized with respect to the solute surface by minimizing the solvent energy while fixing the solute moiety. Then solvent molecules are thermalized at the simulation temperature (300 K) by running dynamics with the solute fixed. A scaled harmonic constraint potential in the buffer region acts as the boundary potential for the protein moiety and keeps the structural integrity of the complex. The solvated complex system is further equilibrated for 10ps and the SBMD simulation is performed for 10ps, from which the dynamics trajectory is obtained for conformational analyses.

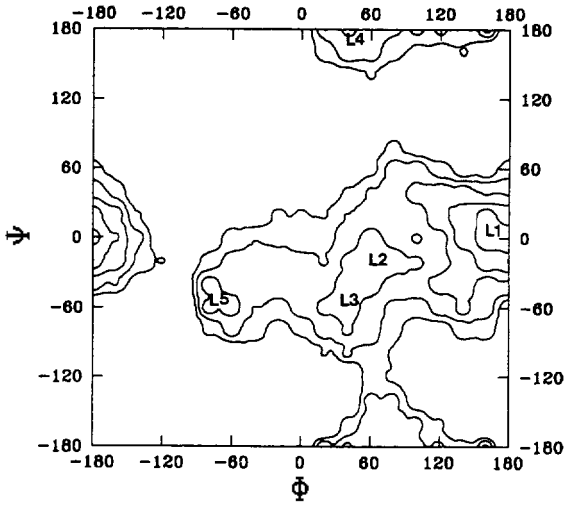

Figure 3. Adiabatic energy map of lactose generated *in vacuum* (ε = 1.0). Contours are in 2 kcal/mole intervals from 2.0 to 10.0 kcal/mole above the energy minimum. Five low-energy conformers of lactose are labeled as L1 through L5.

Results and Discussion

Adiabatic Energy Map. Figure 3 is the adiabatic potential energy map of lactose generated *in vacuum* (ε = 1.0). It shows five local minima corresponding to relatively low-energy conformations of lactose, which are designated as L1, L2, L3, L4, and L5, respectively.

The dominant structure on the map is the RR conformation, where the former R denotes the intraring hydrogen bonding pattern of galactose and the latter does the intraring hydrogen bonding pattern of glucose. While as the potential energy of D-glucose with the C form is about 4 kcal/mole higher than that of D-glucose with the R form, the potential energy of D-galactose with the C form is similar to that of

Table 3. Conformational features and relative energy of the minimum energy conformations found on the vacuum energy map

	NMR[a] (free)	NMR[a] (bound)	Crystal[b] (free)	Crystal[c] (free)	L1	L2	L3	L4	L5
H1'-C1'-O4-C4	59	51	52.0	33.2	164.8	64.4	34.0	45.8	−66.9
C1'-O4-C4-H4	−7	−5	−7.6	−27.5	1.8	−17.4	−62.4	171.3	−66.2
O5'-C5'-C6'-O6'			50.5	58.3	45.6	41.6	50.9	55.8	47.8
O5-C5-C6-O6			72.6	63.4	−50.9	45.1	43.6	70.2	43.1
H1'-H4	2.4	2.2	2.4		3.5	2.4	2.4	3.7	3.3
ENERGY[d]					0.0	4.93	5.56	5.62	5.59

[a] Reference 6. [b] Reference 25. [c] Reference 26. [d] in kcal/mol, relative to the global minimum L1.

D-galactose with the R form. Therefore, the CR structure can be found as the minimum energy conformation at some grid points, and RC and CC conformations are not found on the map.

The data in Table 3 indicate that the GT exocyclic conformation is the dominant form in both glucose and galactose moieties. Table 3 also lists a set of selected torsion angles and the H1'-H4 distance of the low energy conformers of lactose located on the vacuum energy map. It is clear that distance information relating the anomeric proton of galactose, H1' to transglycosidic glucose protons such as H3, H4, and H5 would be of major interest. The H4 proton shows strong nOe to the H1' proton in both free and bound forms. These low energy structural values are compared to the experimental data. Note that the solution NMR structure and the X-ray crystallographic structure of lactose are close to the L2 conformation. The experimentally determined H1'-H4 distance constraint is satisfied only in the region near L2 and L3.

L1 at $\phi = 164.8°$ and $\psi = 1.8°$ is the lowest energy conformation *in vacuum* and the conformation is characterized as GTGG-RR, where GT denotes the exocyclic hydroxyl conformation of the galactose moiety, GG is used for that of the glucose moiety, and RR denotes the intraring hydrogen bonding patterns. The H1'-H4 distance of L1 is 3.5 Å, longer than that of the experimentally determined structures. L1 has two interring hydrogen bonds, O6···HO6'-O6' with the O6-HO6' distance of 1.95 Å and O3···HO2'-O2' with the O3-HO2' distance of 1.95 Å. The interring hydrogen bonds are the dominant structural factors in constructing the lowest energy conformation *in vacuum*. Here, no solvent effect is incorporated into the map calculation and it is not surprising to have the most stable conformation different form that determined by the X-ray crystallography and the NMR experiment.

The other local minima L2 through L5 are all characterized as GTGT-RR. L2 at $\phi = 64.0°$ and $\psi = -17.4°$ has the interring hydrogen bond O3···HO6'-O6' with the O3-HO6' distance of 1.92 Å and its H1'-H4 distance is 2.4 Å. Even though L2 is not the global minimum conformation, it is close to the experimentally observed structure. Another local minimum structure, L3 at (34.0°-62.4°, also shows the H1'-H4 distance of 2.4 Å. L4 at (−46.0°, 171.3°) has the H1'-H4 distance of 3.7 Å and the O6···HO6'-O6' interring hydrogen bond with the O6-HO6' distance of 2.0 Å. L5 at (−66.9°, −66.2° has the H1'-H4 distance of 3.3 Å and the O3···HO2'-O2' interring hydrogen bond with the O3-HO2' distance of 1.84 Å.

A map generated with constrained values of Φ and Ψ but optimized in all other degrees of freedom is called a relaxed map,[9,24] against the rigid map which is generated with some degrees of freedom, normally bond lengths and bond angles, fixed. Because all internal degrees of freedom are allowed to relax, the relaxed map contains expanded contours around minima as compared to those on rigid map. While the van der Waals energy makes a dominant contribution in the rigid map, the sum of the electrostatic energy, the dihedral energy and the van der Waals energy constructs the contour pattern of the relaxed map. The electrostatic energy contribution is important in the relaxed energy map and the dielectric insulation of aqueous solvent can be effectively introduced

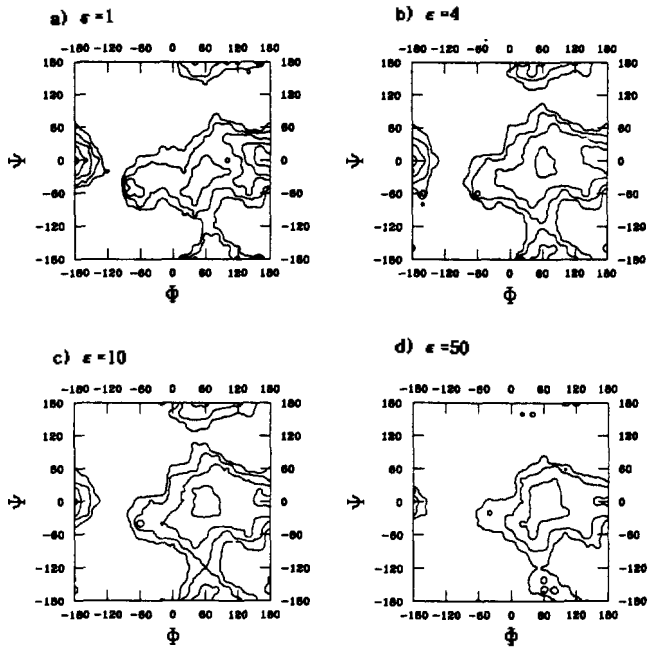

Figure 4. Adiabatic energy map of lactose with setting the dielectric constant to (a) $\varepsilon = 1.0$, (b) $\varepsilon = 4.0$, (c) $\varepsilon = 10.0$, and (d) $\varepsilon = 50.0$.

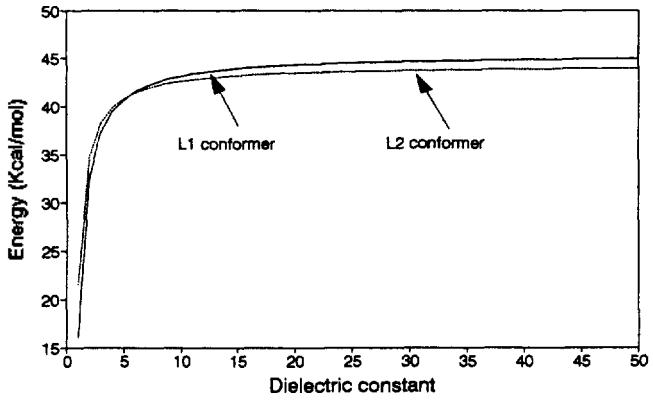

Figure 5. Potential energy of the L1 and L2 conformers as a function of the dielectric constant.

through the dielectric constant. All the energy maps shown in this paper are the relaxed maps.

Energy maps are generated with the dielectric constant of 4.0, 10.0 and 50.0 and shown in Figure 4 (b) through (d), respectively. The vacuum energy map with $\varepsilon = 1.0$ is also shown in Figure 4(a) for comparison. Since solvent-solute interactions are strong in the aqueous solution of lactose, intramolecular hydrogen bonds are weakened and replaced with solvent-solute hydrogen bonds. The increased dielectric insulation effectively makes intraring hydrogen bonds weaker than those *in vacuum* and results in a feasible structure in solution.

While the global minimum L1 of the vacuum energy map becomes one of the local minima on the dielectric energy maps, the L2 conformation becomes the lowest energy conformation as the dielectric constant gets larger than approximately 5.0. Figure 5 shows the conformation energies of L1

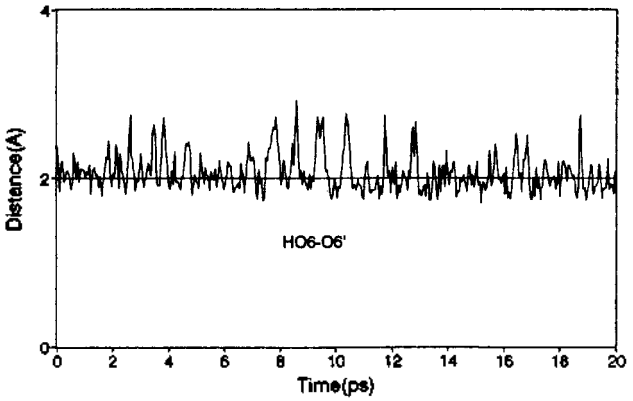

Figure 6. The O6'-HO6'···O6 hydrogen bond distance of the L1 trajectory generated *in vacuum*.

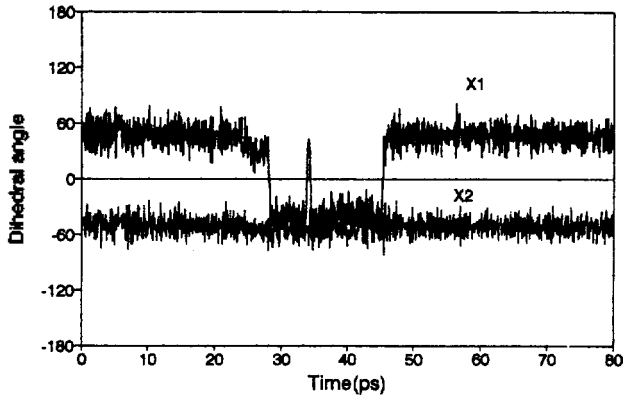

Figure 7. The exocyclic dihedral angle χ_1 (O5'-C5'-C6'-O6') and χ_2 (O5-C5-C6-O6) of the L1 trajectory generated *in vacuum*.

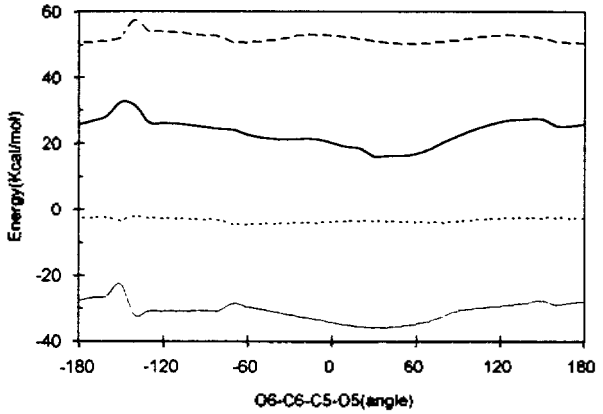

Figure 8. The potential energies as a function of the exocyclic dihedral angle χ_1 (O5'-C5'-C6'-O6') of the L1 conformation *in vacuum*.: the dihedral energy (---), the electrostatic energy (—), the van der Waals energy (···), and the total energy (—).

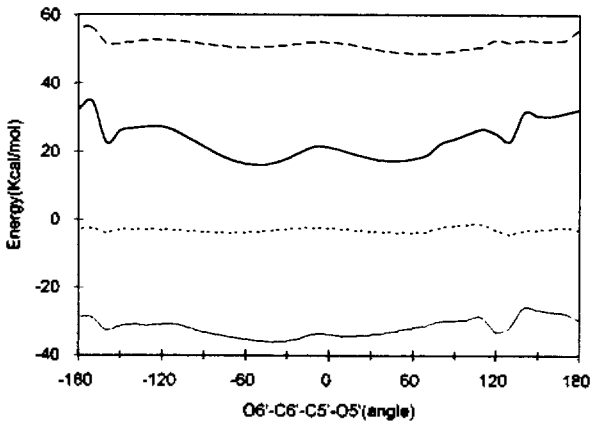

Figure 9. The potential energies as a function of the exocyclic dihedral angle χ_2 (O5-C5-C6-O6) of the L1 conformation *in vacuum*.: the dihedral energy (---), the electrostatic energy (—), the van der Waals energy (···), and the total energy (—).

and L2 as a function of the dielectric constant. As shown in the figure, L1 is more stable than L2 *in vacuum*. However, the energy of L1 increases more rapidly than that of L2 as the dielectric constant increases. After the intersection at 5.5, the energy of L2 becomes lower than that of L1 and the potential energy becomes constant as the dielectric constant increases beyond 15.0. The L2 structure obtained with $\varepsilon=50.0$ reproduces the structural constraints determined by the X-ray crystallographic and the NMR experiments.

Molecular Dynamics Simulation. Dynamic behavior of the lactose molecule on the adiabatic potential surface is examined through a set of molecular dynamics simulations. The initial atomic coordinates for each simulation are taken from one of five minimum conformations on the energy map. The dynamics trajectory is generated by following the standard dynamics procedure of the heating-equilibrium-production protocol as described in the theory section. As previously noted, the entire trajectory including the heating phase is monitored with paying special attentions to conformational transitions.

The trajectory initiated from the L1 conformation is designated as the "L1 trajectory" in our discussion. The L1 trajectory generated *in vacuo* includes no transition to other local minima but shows fluctuations around the L1 conformation in some degree. As shown in Figure 6, the interring hydrogen bond, O6···HO6'-O6' is maintained throughout the entire L1 trajectory. The other interring hydrogen bond, O3···HO2'-O2', is also maintained. During the MD simulation, the intraring hydrogen bonding pattern is also retained. The exocyclic hydroxymethyl group of the galactose moiety (χ_1) undergoes transitions between GT and GG, but that of glucose (χ_2) does not make transitions as shown in Figure 7. Although the GT-GG transition is observed after 10.5 ps during the MD simulation, the O6···HO6'-O6' hydrogen bond is not broken and the overall feature of the L1 conformation is retained.

Because the interring hydrogen bond is directly related to the orientation of the exocyclic hydroxymethyl groups, it is important to examine the conformational energy with rotating the exocyclic hydroxymethyl group. The rotational energy of the exocyclic hydroxymethyl group is calculated with incrementing the exocyclic angle by 10° and subsequently minimizing the exocyclic constrained structure. All degrees of freedom except the exocyclic angles are relaxed. The L1 conformation which is the global minimum structure *in vacuum* is used as an initial structure. Figure 8 shows

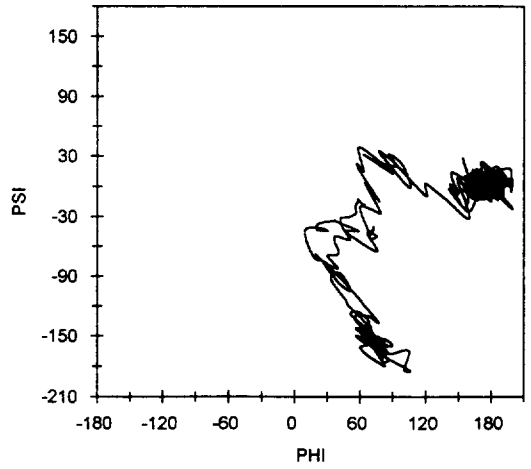

Figure 10. The L2 trajectory generated *in vacuum* on the (ϕ, ψ) plane.

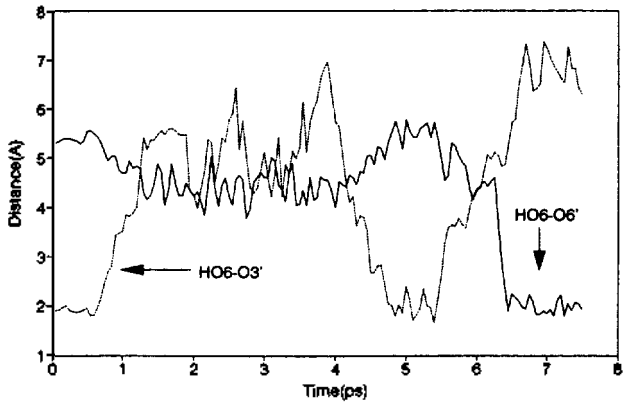

Figure 11. The O3···HO6'-O6' and O6···HO6'-O6' hydrogen bond distances of the L2 trajectory.

the potential energy as a function of the exocyclic angle χ_1 (O6'-C6'-C5'-O5') together with contributions of the dihedral, van der Waals and electrostatic energy terms. There is no significant barrier between the GG (−60.0°) and GT (+60.0°) conformations and the GG $\rightleftarrows$ GT transition can easily take place. Note that the dihedral energy barrier at χ_1=0.0° makes little contribution to the total energy. As there is the significant barrier between GT and TG (+180.0°, transitions between these conformations are not observed. Figure 9 is the result of the similar calculation showing the potential energy and energy terms as a function of the exocyclic angle χ_2 (O6-C6-C5-O5). The figure shows the relatively high rotational barrier between the GG and GT conformations.

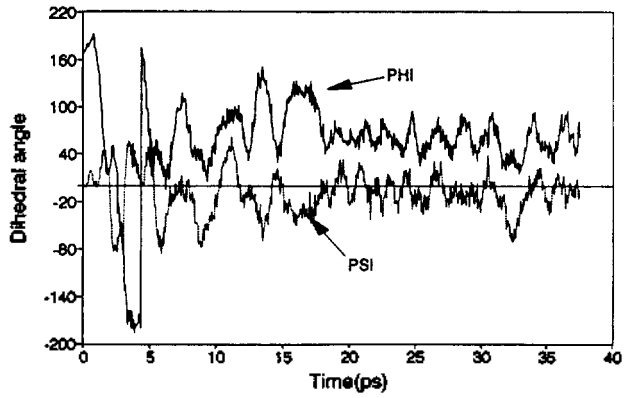

Figure 12. The glycosidic dihedral angles Φ and Ψ of the L1 trajectory generated with the dielectric constant of 50.

The L2 trajectory ends up with the L1 conformation. The transition pathway, L2-L3-L4-L3-L2-L1, is shown in Figure 10. Figure 11 shows the O3···HO6'-O6' and O6···HO6'-O6' distances of the L2 trajectory as a function of the simulation time. The former is broken at 1 ps and recovered for a while around at 5 ps. After 6.5 ps, the transition to L1 takes place as the O6···HO6'-O6' hydrogen bond forms. The L3 trajectory shows a dynamic trend shifting toward the L4 conformation. The L4 and L5 trajectories include no transition to other conformations. Dihedral angles (ϕ, ψ, χ_1 and χ_2) and the H1'-H4 distance obtained from each averaged dynamics trajectories are summarized in Table 4.

As in the energy map calculation, effects of the aqueous solvent can be incorporated into molecular dynamics simulations by increasing the dielectric constant. With setting the dielectric constant to 50.0, the same set of molecular dynamics simulations have been carried out. Because increased dielectric shielding weakens intramolecular electrostatic interactions, there no longer appears the intramolecular hydrogen bonding pattern (C or R) around the ring. Dielectric insulation suppresses electrostatic interactions and thus results in more flexible molecular conformations.

In contrast to the vacuum dynamics, the L1 trajectory generated with ε=50.0 has the transition to the L2 conformation. The glycosidic dihedral angles extracted from the L1 trajectory are plotted as a function of the simulation time in Figure 12. It shows a large amplitude fluctuation in ψ at the beginning and indicates that the transition takes place at around 6.5 ps and the new conformation is stabilized by 20 ps. The interring hydrogen bond O6···HO6'-O6' is monitored from the beginning of the trajectory. Figure 13 indicates that the hydrogen bond holds upto 1.5 ps and is broken by 3 ps. The exocyclic hydroxymethyl group of the galactose moiety

Table 4. Conformational features obtained from averaged dynamics trajectories generated *in vacuum*

	L1	L2	L3	L4	L5
H1'-C1'-O4-C4	163.3 (± 8.9)	172.0 (± 8.5)	74.3 (± 10.1)	62.9 (± 18.0)	−67.6 (± 10.8)
C1'-O4-C4-H4	2.8 (± 8.3)	0.4 (± 8.4)	−156.0 (± 9.4)	−157.8 (± 14.6)	−65.8 (± 9.9)
O5'-C5'-C6'-O6'	32.0 (± 33.4)	58.6 (± 10.5)	−29.8 (± 28.4)	31.3 (± 37.7)	47.9 (± 8.7)
O5-C5-C6-O6	−51.0 (± 8.7)	38.5 (± 27.6)	26.7 (± 33.3)	2.9 (± 41.6)	32.5 (± 28.2)
H1'-H4	3.52 (± 0.08)	3.55 (± 0.08)	3.57 (± 0.12)	3.6 (± 0.12)	3.3 (± 0.98)

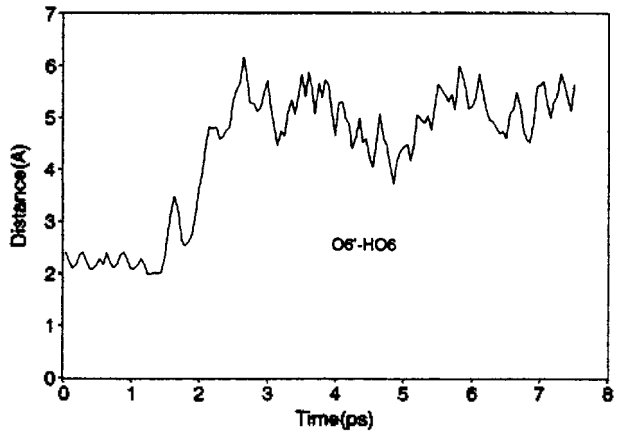

Figure 13. The O6···HO6'-O6' hydrogen bond distance of the L1 trajectory generated with the dielectric constant of 50.

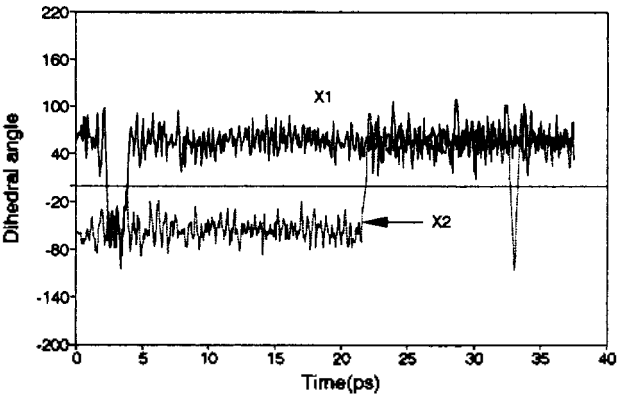

Figure 14. The dihedral angles χ_1 (O5'-C5'-C6'-O6') and χ_2 (O 5-C5-C6-O6) of the L1 trajectory generated with the dielectric constant of 50.

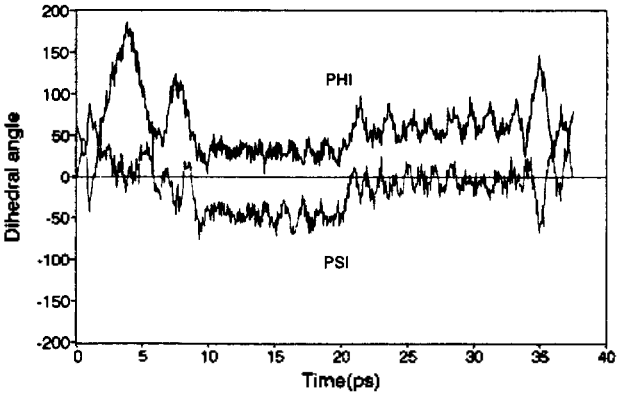

Figure 15. The glycosidic dihedral angles Φ and Ψ of the L2 trajectory generated with the dielectric constant of 50.

makes transitions between GT and GG and that of the glucose moiety undergoes transition from GG to GT as shown in Figure 14. The increased dielectric shielding also makes the exocyclic hydroxymethyl transitions easier than *in vacuum*.

As the dielectric constant increases, the region near L2

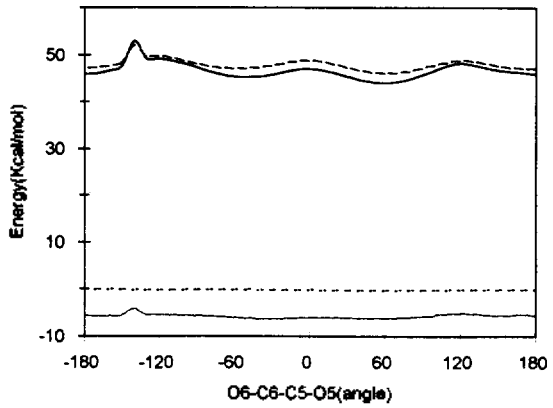

Figure 16. The potential energies as a function of the exocyclic angle χ_1 (O5'-C5'-C6'-O6') of the L2 conformation with the dielectric constant set to 50.: the dihedral energy (---), the electrostatic energy (—), the van der Waals energy (···), and the total energy (—).

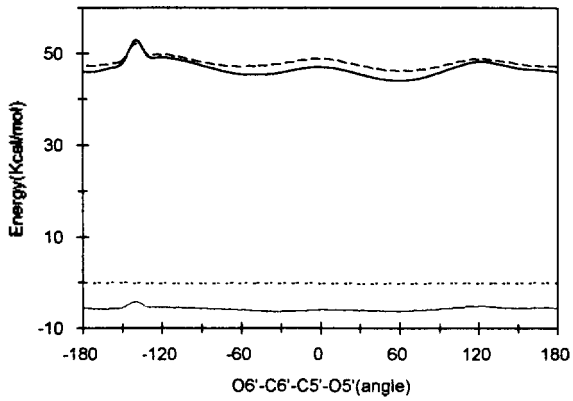

Figure 17. The potential energies as a function of the exocyclic angle χ_2 (O5-C5-C6-O6) of the L2 conformation with the dielectric constant set to 50.: the dihedral energy (---), the electrostatic energy (—), the van der Waals energy (···), and the total energy (—).

and L3 becomes the global minimum in the adiabatic energy maps shown in Figure 4. The lowest energy conformation L2 does not evolve into other local minima as shown in Figure 15. While no transition is observed in the L2 trajectory, Figure 15 displays ϕ and ψ fluctuations in larger amplitude compared to those observed during the vacuum dynamics simulation.

The potential energy and the dihedral, van der Waals and electrostatic energy contributions of the L2 conformer are calculated as a function of the exocyclic angle χ_1 (O6'-C6'-C5'-O5') and shown in Figure 16. The dielectric constant of 50.0 effectively suppresses any significant electrostatic interactions and makes the dihedral energy be the major contributor to the rotational barrier. The same is observed for the glucose exocyclic angle χ_2 (O6-C6-C5-O5) rotation shown in Figure 17. Along the L2 trajectory, χ_1 makes transitions between GG and GT and χ_2 makes GG-GT-TG transitions as shown in Figure 18. Note that the transition to TG is not observed in the vacuum simulation due to the relatively

Table 5. Conformational features obtained from averaged dynamics trajectories generated with the dielectric constant of 50

	L1	L2	L3	L4	L5
H1'-C1'-O4-C4	68.3(± 22.1)	59.7(± 22.1)	39.4(± 10.7)	58.8(± 18.1)	73.5(± 22.0)
C1'-O4-C4-H4	−3.4(± 18.2)	−11.6(± 21.6)	175.7(± 7.2)	−167.8(± 13.3)	−26.4(± 15.8)
O5'-C5'-C6'-O6'	22.9(± 51.1)	44.6(± 37.9)	58.9(± 10.9)	62.1(± 12.8)	57.4(± 12.1)
O5-C5-C6-O6	53.1(± 17.6)	70.4(± 103.8)	61.1(± 11.0)	23.6(± 51.5)	56.6(± 13.5)
H1'-H4	2.59(± 0.32)	2.50(± 0.27)	3.64(± 0.08)	3.61(± 0.11)	2.54(± 0.29)

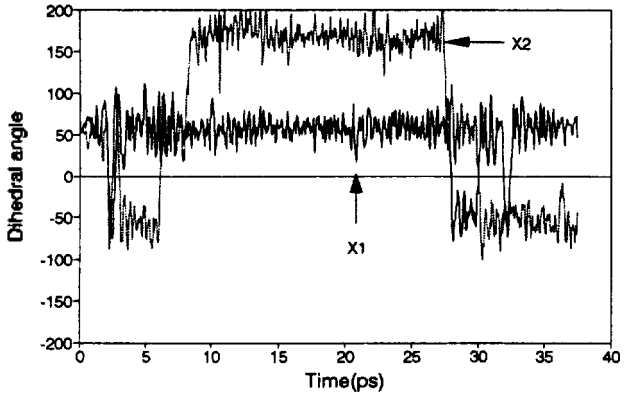

Figure 18. The exocyclic dihedral angles χ_1 (O5'-C5'-C6'-O6') and χ_2 (O5-C5-C6-O6) of the L2 trajectory generated with the dielectric constant of 50.

high energy barrier in Figure 7. Figure 18 does not show a direct transition between GG to TG conformations, which reflects the barrier between them shown in Figure 17.

The L3 trajectory undergoes shifting toward the L4 conformation. The L4 trajectory includes no significant transitions to other conformations. The L5 conformation evolves into the lowest energy conformation L2 along the simulated trajectory. Dihedral angles (ϕ, ψ, χ_1 and χ_2) and the H1'-H4 distance are averaged out of each dynamics trajectory generated with $\varepsilon=50.0$, which are summarized in Table 5.

Explicit water molecules are introduced as the solvent and the constant dielectric electrostatic option with $\varepsilon=1.0$ is employed in the SBMD simulation. Simulations have been carried out separately for each binding site, and the dynamics trajectory is monitored during the 10ps run with the equilibrated system. The dynamical mean structures averaged from the trajectories are summarized in Table 6. Both of the dynamics trajectories fluctuate around the conformation corresponding to the global minimum on the adiabatic energy map with the dielectric constant larger than 10.0.

The dynamics average H1'-H4 distance is 2.29± 0.14 Å for the lactose at the binding site 1 and 2.25± 0.14 Å for the lactose at the site 2. The binding structure of lactose is close to the L2 conformation, which is the most stable one in a dielectric aqueous medium. Table 3 lists the H1'-H4 distance of all possible local minimum conformations. The NMR data obtained from the 1D and 2D nOe experiments show that the H1'-H4 distance of the free lactose is 2.36 Å and that of the bound lactose is 2.22 Å.[6] The NMR data indicate that there is a minor change in the glycosidic torsion angle upon binding and the change leads to the decrease

Table 6. Conformational features obtained from averaged SBMD trajectories of the lactose-ricin B chain complex system

	Site 1	Site 2
H1'-C1'-O4-C4	41.8 (± 13.0)	42.7 (± 8.8)
C1'-O4-C4-H4	−46.5 (± 11.5)	−25.0 (± 9.8)
O5'-C5'-C6'-O6'	57.1 (± 8.8)	−66.0 (± 7.9)
O5-C5-C6-O6	28.3 (± 59.2)	−69.3 (± 16.4)
H1'-H4	2.29 (± 0.14)	2.25 (± 0.14)

of the H1'-H4 distance. The dynamics average structures of the lactose bound to the ricin B chain show that the H1'-H4 distance agrees well with that of the NMR structure obtained for the bound lactose. The agreement strongly indicates the validity of the SBMD model system and suggests that the most stable lactose conformation in solution is also found at the binding sites of the ricin B chain.

While the trajectory of the lactose bound to the site 1 is averaged to yield the structure close to that of the L2 trajectory produced with $\varepsilon=50.0$, the exocyclic hydroxymethyl groups of the lactose at the site 2 assume orientations quite different from those found in the L2 trajectory. The different dynamical behavior with respect to the exocyclic orientation reflects the fact that the two binding sites have different molecular construction and the binding affinity to lactose is slightly different. The SBMD simulation shows that the binding conformations of lactose to both binding sites are similar and some adjustments are made in the peripheral moiety, *i.e.*, exocyclic hydroxymethyl groups.

Conclusions

Combined usage of the adiabatic energy map and molecular dynamics simulations has been applied to studying conformational details of lactose binding to the ricin B chain. The adiabatic energy map reveals that lactose can exist with a variety of conformational flexibility. While the lowest energy structure (L1) in the vacuum adiabatic energy map has the glycosidic dihedral angles of $\Phi=164.8°$ and $\Psi=1.8°$, the lowest energy structure (L2) in the adiabatic energy map generated with the dielectric constant of 50.0 has $\Phi=61.0°$, $\Psi=-3.0°$. The global minimum structure obtained by setting the dielectric constant to 50.0 agrees with the experimental structure observed by NMR and X-ray crystallography. The L2 structure is also observed during the solution phase SBMD simulation of the lactose and ricin B complex.

Since the electrostatic interactions are reduced in dielectric media, the aqueous environment in solution and *in vivo*

enhances molecular flexibility of a charged and/or polar solute molecule as compared to that *in vacuum*. The simulations carried out in this work have demonstrated that dielectric shielding of solvent molecules can be effectively mimicked by applying an increased dielectric constant to the molecular model system. Although it is not possible to evaluate quantitatively the exact value of the dielectric constant representing an aqueous solution, it would be appropriate to replace explicit water molecules working as the solvent by the dielectric constant larger than 10.0. The increased dielectric constant in the potential energy function suppresses overemphasized electrostatic energy terms, including hydrogen bond strength, and removes intramolecular strain imposed by nonbonded interactions, which is what solvent molecules do in effect.

According to the NMR study on conformational behavior of the lactose molecule, there is some structural changes of the lactose upon binding to the ricin B chain: the glycosidic torsion angle Φ by $-8.0°$, Ψ by $+2°$ and the H1'-H4 distance by -0.2 Å. Both of the free and the bound conformation are located at around the L2 region on the "in aquo" energy map generated with $\varepsilon>10.0$. Solvent molecules play a key role in making the substrate molecule be flexible enough and take suitable conformation for binding to the receptor. The most stable conformation in solution is picked up into the binding sites of the ricin B chain and conformational modification or fitting into the binding site is accomplished through adjustments in exocyclic hydroxymethyl orientations.

Acknowledgment. This work was supported by the Korea Science and Engineering Foundation (YK, 931-0300-031-2) and by the Basic Science Research Institute Program, Ministry of Education of Korea (BSRI-94-3428).

References

1. Howard, M. E. Transactions of the American crystallographic association. **1989**, 25.
2. Kornfeld, K.; Reitman, M. L.; Kornfeld, R. *J. Biol. Chem.* **1981**, *256*, 6633.
3. Houston, L. L.; Dooley, T. P. *J. Biol. Chem.* **1982**, *257*, 4147.
4. Rutenber, E.; Robertus, J. D. *Proteins; struct., Funct., Genet.* **1991**, *10*, 260.
5. Yamasaki, N.; Hatakeyama, T.; Funatsu, G. *J. Biochem.* **1985**, *98*, 1555.
6. Bevilacqua, V. L.; Thomson, D. S.; Prestegard, J. H. *Biochemistry* **1990**, *29*, 5529.
7. Bevilacqua, V. L.; Kim, Y. M.; Prestegard, J. H. *Biochemistry* **1992**, *31*, 9339.
8. Rees, D. A.; Morris, E. R.; Thom, D.; Madden, J. K. in The Polysaccharides, Vol. 1, Aspinall, G. O., Ed., Academic, New York, 1982, 195.
9. Gelin, B. R.; Karplus, M. *J. Am. Chem. Soc.* **1975**, *97*, 6996.
10. Joshi, N. V.; Rao, V. S. *Biopolymers* **1979**, *18*, 2993.
11. Cumming, D. A.; Carver, J. P. *Biochemistry* **1987**, *26*, 6664.
12. Brady, J. W. *J. Am. Chem. Soc.* **1986**, *108*, 8153.
13. Brady, J. W. *Carbohyd. Res.* **1987**, *165*, 306.
14. Tran, V.; Vuleon, A.; Imberty, A.; Pérez, S. *Biopolymers* **1989**, *28*, 679.
15. Brooks, S. R.; Bruccoleir, R. E.; Olafson, B. D.; States, D. J.; Swaminathan, S.; Karplus, M. *J. Comput. Chem.* **1983**, *4*, 187.
16. CHARMm version 22 all hydrogen parameter set, CARBOH.RTF and CARBOH.PRM.
17. Molecular Simulations Inc., 16 New England Executive Park, Burlington, MA 01803, U.S.A.
18. Born, M.; Von Karman, *Physik. Z.* **1912**, *13*, 297.
19. Brooks III, C. L.; Brünger, A.; Karplus, M. *Biopolymer*, **1985**, *24*, 845.
20. Jorgensen, W. L.; Chandrasekhar, J.; Madura, J. D.; Impey, R. W.; Klein, M. L. *J. Chem. Phys.* **1983**, *79*, 926.
21. Stillinger, F. H.; Rahman, A. *J. Chem. Phys.* **1974**, *60*, 1545.
22. Ha, S. N.; Madsen, L. J.; Brady, J. W. *Biopolymers* **1988**, *27*, 1927.
23. Verlet, L. *Phys. Rev.* **1967**, *159*, 98.
24. French, A. D. *Biopolymers* **1988**, *27*, 1519.
25. Hirotsu, K.; Shimada, A. *Bull. Chem. Soc. Jpn.* **1974**, *47*, 1872.
26. Noordick, J. H.; Beurskens, P. T.; Bennema, P.; Bisser, R. A.; Gould, R. O. *Z. Kristallogr.* **1984**, *168*, 59.